Optics Letters

Phase-locking transition in Raman combs generated with whispering gallery mode resonators

Guoping Lin[1,2,*] and Yanne K. Chembo[1]

[1]Optics Department, FEMTO-ST Institute, CNRS & Université Bourgogne-Franche-Comté, 15B Avenue des Montboucons, 25030 Besançon cedex, France
[2]MOE Key Laboratory of Fundamental Physical Quantities Measurement, School of Physics, Huazhong University of Science and Technology, 1037 Luoyu Road, Wuhan 430074, China
*Corresponding author: guoping_lin@hust.edu.cn

Received 9 May 2016; revised 30 June 2016; accepted 8 July 2016; posted 11 July 2016 (Doc. ID 264747); published 3 August 2016

We investigate the mechanisms leading to phase locking in Raman optical frequency combs generated with ultrahigh Q crystalline whispering gallery mode disk resonators. We show that several regimes can be triggered depending on the pumping conditions, such as single-frequency Raman lasing, multimode operation involving more than one family of cavity eigenmodes, and Kerr-assisted Raman frequency comb generation. The phase locking and coherence of the combs are experimentally monitored through the measurement of beat signal spectra. These phase-locked combs, which feature high coherence and wide spectral spans, are obtained with pump powers in the range of a few tens of mW. In particular, Raman frequency combs with multiple free-spectral range spacings are reported, and the measured beat signal in the microwave domain features a 3 dB linewidth smaller than 50 Hz, thereby indicating phase locking. © 2016 Optical Society of America

OCIS codes: (140.4780) Optical resonators; (140.3550) Lasers, Raman; (190.5650) Raman effect; (190.3270) Kerr effect; (190.4380) Nonlinear optics, four-wave mixing.

http://dx.doi.org/10.1364/OL.41.003718

Stimulated Raman scattering (SRS) is a fundamental inelastic scattering process that results from the interaction between light and molecular vibrations. SRS is generally exploited for laser generation and optical frequency conversion at new wavelengths in various transparent media. However, the required operation intensity of the pump laser is usually very high. Therefore, optical cavities have been used to achieve low-threshold Raman lasing in the continuous-wave (CW) regime. For instance, on-chip race track resonators have been used to realize CW Raman lasers in silicon [1].

Whispering gallery mode (WGM) resonators are capable of confining light within a small volume for a long lifetime scale (>1 μs). They have become ideal platforms for investigating nonlinear scattering phenomena [2], including Raman amplification and lasing. Light in such resonators is trapped by successive total internal reflections along a circular boundary. With a low-loss host material and a suitable axisymmetric geometry, WGMs can easily feature an ultrahigh quality (Q) factor above 10^8 [3–5]. Low-threshold CW Raman lasing has been demonstrated in different silica WGM resonators, including microspheres [6], microtoroids [7], microbubbles, and microbottles [8,9]. CW WGM Raman lasing has also been reported in other materials such as coated polymers [10], chalcogenides [11,12], lithium niobate [13], and calcium fluoride [14–17]. In recent years, nanoparticle sensor applications based on such lasers have been reported [18,19], and anti-Stokes Raman lasing has been observed [20].

Besides Raman lasing, Kerr-assisted Raman lasing or Raman-assisted four-wave mixing (FWM) also occurs in WGM resonators [6,15–17]. It is a process that involves both SRS gain and Kerr nonlinearity. Since the latter one can lead to the generation of optical frequency combs [21], Raman lasing and Kerr frequency comb generation can compete with each other. As a result, Raman-assisted FWM is usually observed in the normal dispersion regime where the direct generation of a Kerr frequency comb is difficult.

In this Letter, we investigate the mechanisms leading to phase locking in Raman optical frequency combs generated with an ultrahigh Q BaF_2 whispering gallery mode disk resonator. Other states such as single-mode Raman lasing and unstable multimode Raman lasing are evidenced as well. A discontinuous step in the resonator transmission of the pump signal was found to coincide with the transition from single-mode lasing to phase-locked multimode lasing. Moreover, we also demonstrate a Raman comb with frequency spacing of triple free-spectral range (FSR). The measured 3 dB linewidth of its beat note at 16.4 GHz was less than 50 Hz, which confirms its phase-locked state. Such Kerr-assisted Raman lasers can find potential applications in the fields of sensors and photonic microwave generation.

The BaF_2 crystalline WGM resonator was fabricated using a mechanical polishing method. Its Q-factors can reach one billion at telecommunication wavelengths [22]. The experimental setup is illustrated in Fig. 1. A CW fiber laser with sub-kHz linewidth was used as the pump source at the 1550 nm band. Its wavelength is tunable through a piezoelectric modulation input. A Pound–Drever–Hall (PDH) locking method was

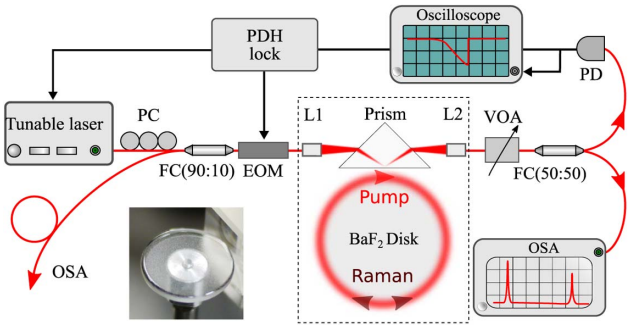

Fig. 1. Schematic illustration of the experimental setup for the WGM Raman laser characterization. PDH, Pound–Drever–Hall locking; PC, fiber polarization controller; FC, fiber directional coupler; EOM, electro-optic modulator; L1,L2, GRIN lenses; VOA, variable optical attenuator; OSA, optical spectrum analyzer; PD, photodetector.

utilized to further lock the pump wavelength to selected WGM resonances. The laser polarization can be optimized using a fiber polarization controller (PC). A directional fiber coupler (FC) extracted 10% of the backward light to monitor its optical spectrum. A fast photodiode with an electrical spectrum analyzer (ESA) can then be used to examine the beat signals in the microwave domain. An electro-optical phase modulator (EOM) was inserted to generate sidebands for PDH locking. The light coupling into the disk resonator was achieved by using an SF11 glass prism which has a higher refractive index than BaF_2. Two fiber GRIN lenses focused the light into the backside of the prism and back into a single-mode fiber. The disk resonator was mounted on a 3D stage, where a piezoelectric actuator was inserted to finely control the coupling gap between the prism and the disk. The power of the transmitted signal through the prism coupling setup was controlled using a variable optical attenuator. The output signal was then split by a 3 dB fiber coupler into a high-resolution optical spectrum analyzer (APEX OSA) and a photodiode to provide the input signal for the PDH locking.

We have previously shown that Brillouin lasing can be realized in such high-Q centimeter scale disk resonators, despite the very narrow bandwidth of stimulated Brillouin scattering gain in BaF_2 crystal [23]. Thereby, the SRS gain which has a much wider gain bandwidth can be more easily used to achieve Raman lasing in such resonators, since the doubly resonant enhancement can be easier to realize. Moreover, the BaF_2 disk is characterized by a normal dispersion at telecom wavelengths [24], which makes it impossible to achieve Kerr frequency comb generation and helps to trigger Raman lasing instead. To observe Raman lasing in a BaF_2 disk resonator, one has to first tune the pump laser wavelength into a high-Q-factor WGM resonance. Figure 2(a) shows a transmission of a BaF_2 disk resonator with a diameter of 11.9 mm. The pump laser frequency is scanned across the resonance at the speed of 0.76 GHz/s. A broadened resonance shape is observed due to the thermal bi-stability phenomenon in WGM resonators [25]. The negative thermo-optic coefficient of BaF_2 (-16×10^{-6}/K) [26] results in the fact that the broadened shape is often observed at the blue scanning side of the laser ramping. Since the thermo-optic and thermal expansion effects have opposite signs, self-thermal oscillations occur [27]. Therefore, it is impossible to apply the self-thermal locking method that

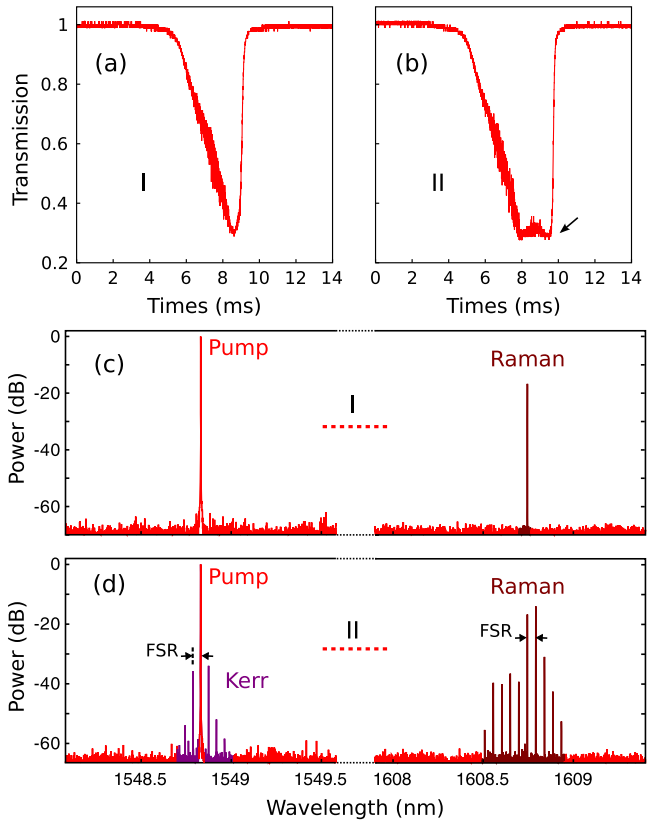

Fig. 2. Distinct regimes in the transmitted WGM signals where the transition from a single-frequency WGM Raman laser to a phase-locked Raman comb occurs. (a), (b) Transmission spectra (labeled as I and II) with slightly different coupling gaps. (c), (d) Raman laser spectra corresponding to the coupling condition I and II, respectively. FSR: 5.5 GHz (47 pm in wavelength at 1608 nm).

has been successfully used in silica resonators [28]. Nevertheless, the PDH locking technique was successfully applied in this experiment. Figure 2(c) shows the corresponding Raman lasing spectrum. A single-mode Raman lasing occurs at 1608.75 nm with its linewidth limited by the resolution of OSA (5 MHz at minimum). Taking into account that the pump wavelength was at 1548.83 nm, we obtained a frequency shift of 7.2 THz, which corresponds to 240 cm^{-1} in the wavenumber unit. This value is in good agreement with the reported SRS frequency shift in BaF_2 [29]. A similar spectrum has also been observed in the backward direction, which is consistent with the fact that Raman lasing occurs in both directions inside the resonator.

To investigate the various dynamical regimes of Raman lasers in a WGM optical resonator, one has to carefully control the coupling condition which includes the incident pump power, the coupled modes, and the coupling gap. We first kept the incident pump power of 17.6 mW unchanged and slightly varied the coupling gap. We observed a discontinuous step in the resonator transmission, as shown in Fig. 2(b), in comparison with Fig. 2(a). By locking the pump laser to the step highlighted by the arrow, the corresponding Raman lasing spectrum is recorded in Fig. 2(d). One clearly notices a multimode lasing behavior. The mode spacing is 5.5 GHz in frequency which matches the expected FSR of the resonator. Moreover, new Kerr frequency components with one FSR spacing are also

observed around the pump wavelength. In the normal dispersion regime, Raman combs can occur without observing these sidebands [16]. Therefore, these sidebands can come from the FWM process between Raman combs and pump. As a result, the Raman comb has higher power than these sidebands. While in the anomalous dispersion regime, Kerr soliton frequency combs can be first generated around the pump, then subsequently trigger a Raman comb (Stokes soliton comb) [30]. As the Kerr effect modifies the refractive index of the material, it will, in turn, interact with the resonance and cause the discontinuity in the transmission. Similar effects have been recently reported in a soliton Kerr frequency comb in MgF_2 [31] and frequency locked Raman solitons in silicon nitride [32]

By further increasing the incident pump power, we also observed unstable regimes of Raman lasers in the disk resonator. Figure 3 shows a multimode Raman lasing spectrum obtained with a pump power of 26.5 mW. The spectral span of Raman- and Kerr-induced components around the pump were expanded. More than 35 frequency lines are observed in the Raman wavelength, and about 20 Kerr frequency lines appear around the pump. The zoom-in covering a 0.3 nm spectral range around 1608.7 nm is given in the inset of Fig. 3(a). The corresponding frequency spacing matches the resonator FSR. It means that they belong to the same family of WGM which share the same field pattern in the transverse direction. These modes have the best spatial mode overlap with the pump. The FWM process in a WGM resonator then created the one-FSR spaced frequency lines around the pump band. Furthermore, we increase the incident pump power to 39.1 mW. A more complex multimode Raman lasing spectrum was obtained, as shown in Fig. 3(b). As one can see in the inset, the zoom-in shows that a second frequency component repeatedly appears within the spectral range of one FSR. It indicates that the pump power has reached the threshold condition of Raman lasing for another WGM family.

Figure 4 shows a Kerr-assisted Raman comb with a frequency spacing of three FSRs. It was obtained by switching to another WGM resonance for pumping. It is worth noting that different WGMs can be selectively excited by controlling

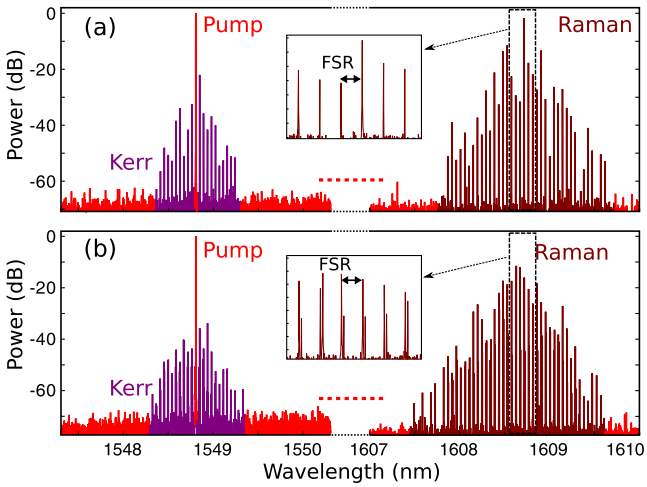

Fig. 3. Multimode WGM Raman laser spectra obtained with higher pump power. (a) Raman laser with only one family of WGM involved, spaced by one FSR. (b) Raman laser with more than one family of WGM involved.

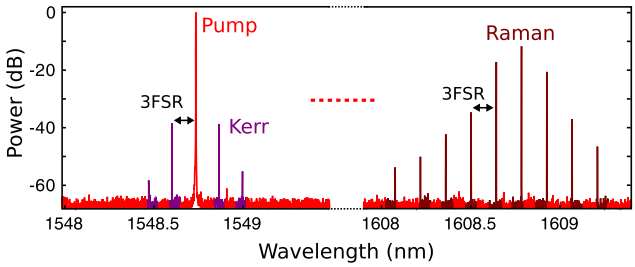

Fig. 4. Phase-locked Kerr-assisted WGM Raman frequency comb spectrum with a frequency spacing matching the triple FSR of the resonator (16.4 GHz or 141 pm at 1608 nm).

either the coupling gap or coupling position along the axial direction [33]. These multi-FSR spacing characteristics are similar to primary Kerr optical frequency combs. Moreover, one expects that this phase locking is dependent on the material dispersion, geometry dispersion, and relative detuning between the pump and the resonance. By choosing different optical modes for pumping, the geometry dispersion can be very different [24] and lead to the observation of such multi-FSR spaced Raman combs.

To further investigate such multimode Raman lasers, we analyze their beat notes in the microwave domain after fast photodetection. Figures 5(a) and 5(b) show the beat notes that correspond to the Raman lasers presented in Figs. 3 and 4, respectively. One can see that the Raman laser operates in an unstable regime when it is overpumped. A beat note at the frequency of 5.468 GHz matching one resonator FSR was then obtained. It should be mentioned that both Raman combs in Figs. 3(a) and 3(b) have the similar beat pattern in the microwave regime. On the other hand, the three-FSR spaced Raman comb was characterized with a beat note that has a much

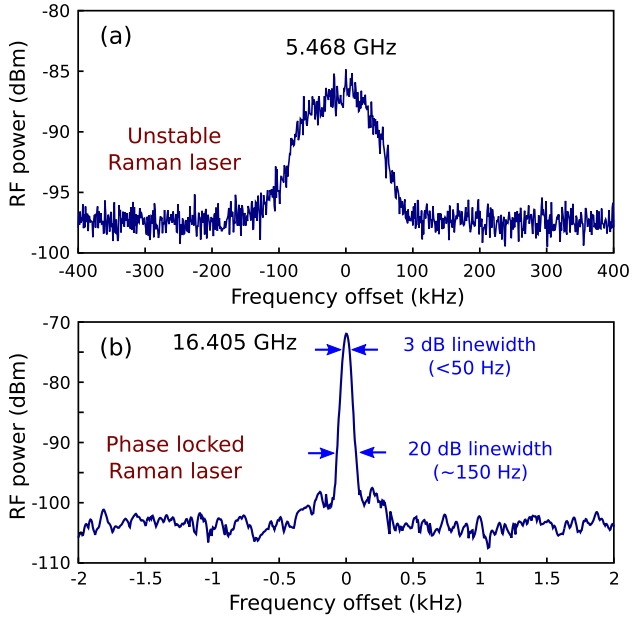

Fig. 5. RF spectra of the beat notes measured by a fast photodiode. (a) Beat spectrum corresponding to the unstable WGM Raman lasers. Resolution bandwidth (RBW), 100 Hz; video bandwidth (VBW), 10 Hz. (b) Beat spectrum corresponding to a phase-locked WGM Raman comb with a three-FSR spacing. RBW, 50 Hz; VBW, 2 Hz.

narrower 3 dB linewidth, typically less than 50 Hz. The measured 20 dB linewidth is as small as 150 Hz. It thereby indicates that a mode-locking mechanism has occurred in this regime. In [16], a mode-locked Raman comb was reported without the observation of the Kerr sideband components around the pump mode. However, we find that the mode-locked regimes can be observed with these frequency components that result from the Raman-assisted FWM. It should be noted that the one-FSR spaced Raman comb shown in Fig. 2(d) also has a similar narrow linewidth beat note. Such phase-locked regimes require specific conditions on the coupling strength and the pump power.

In conclusion, we have investigated the Raman lasing phenomenon in a centimeter scale BaF_2 WGM resonator. We show that dynamic regimes concerning single-mode lasing, mode-locked lasing, and unstable lasing exist in such a Raman laser. We observed the transition between a single-mode Raman laser and a mode-locked Raman laser, which is similar to the observation of a soliton Kerr comb in a crystalline WGM resonator [31]. Furthermore, we report that Raman combs can be achieved with multiple FSR spacing. Such mode-locked Raman lasers can be further applied in sensors and low phase noise microwave oscillators. Recently, a soliton Raman comb has been observed in silica microcavities in the anomalous dispersion regime [30]. Considering the low dispersion profile of BaF_2 in mid-IR [24] and its recently demonstrated high Q-factors around 4.5 μm [34,35], we expect that a Kerr-assisted Raman frequency comb can also be generated in this wavelength regime. Further research will also focus on extreme events [36], chaos [37], and telecommunication performance [38] of these combs.

Funding. European Research Council (ERC) (278616, 632108); Labex ACTION; Centre National d'Etudes Spatiales (CNES); Région de Franche-Comté.

REFERENCES

1. H. Rong, S. Xu, Y.-H. Kuo, V. Sih, O. Cohen, O. Raday, and M. Paniccia, Nat. Photonics **1**, 232 (2007).
2. G. Lin, S. Diallo, J. M. Dudley, and Y. K. Chembo, Opt. Express **24**, 14880 (2016).
3. K. J. Vahala, Nature **424**, 839 (2003).
4. A. B. Matsko and V. S. Ilchenko, IEEE J. Sel. Top. Quantum Electron. **12**, 3 (2006).
5. A. Chiasera, Y. Dumeige, P. Feron, M. Ferrari, Y. Jestin, G. N. Conti, S. Pelli, S. Soria, and G. C. Righini, Laser Photon. Rev. **4**, 457 (2010).
6. S. M. Spillane, T. J. Kippenberg, and K. J. Vahala, Nature **415**, 621 (2002).
7. T. J. Kippenberg, S. M. Spillane, D. K. Armani, and K. J. Vahala, Opt. Lett. **29**, 1224 (2004).
8. D. Farnesi, A. Barucci, G. C. Righini, G. N. Conti, and S. Soria, Opt. Lett. **40**, 4508 (2015).
9. Y. Yang, Y. Ooka, R. M. Thompson, J. M. Ward, and S. N. Chormaic, Opt. Lett. **41**, 575 (2016).
10. B.-B. Li, Y.-F. Xiao, M.-Y. Yan, W. R. Clements, and Q. Gong, Opt. Lett. **38**, 1802 (2013).
11. F. Vanier, M. Rochette, N. Godbout, and Y.-A. Peter, Opt. Lett. **38**, 4966 (2013).
12. F. Vanier, Y.-A. Peter, and M. Rochette, Opt. Express **22**, 28731 (2014).
13. J. Moore, M. Tomes, T. Carmon, and M. Jarrahi, Appl. Phys. Lett. **99**, 221111 (2011).
14. I. S. Grudinin and L. Maleki, Opt. Lett. **32**, 166 (2007).
15. I. S. Grudinin and L. Maleki, J. Opt. Soc. Am. B **25**, 594 (2008).
16. W. Liang, V. S. Ilchenko, A. A. Savchenkov, A. B. Matsko, D. Seidel, and L. Maleki, Phys. Rev. Lett. **105**, 143903 (2010).
17. Y. K. Chembo, I. S. Grudinin, and N. Yu, Phys. Rev. A **92**, 043818 (2015).
18. B.-B. Li, W. R. Clements, X.-C. Yu, K. Shi, Q. Gong, and Y.-F. Xiao, Proc. Natl. Acad. Sci. USA **111**, 14657 (2014).
19. Ş. K. Özdemir, J. Zhu, X. Yang, B. Peng, H. Yilmaz, L. He, F. Monifi, S. H. Huang, G. L. Long, and L. Yang, Proc. Natl. Acad. Sci. USA **111**, E3836 (2014).
20. D. Farnesi, F. Cosi, C. Trono, G. C. Righini, G. N. Conti, and S. Soria, Opt. Lett. **39**, 5993 (2014).
21. P. Del'Haye, A. Schliesser, O. Arcizet, T. Wilken, R. Holzwarth, and T. Kippenberg, Nature **450**, 1214 (2007).
22. G. Lin, S. Diallo, R. Henriet, M. Jacquot, and Y. K. Chembo, Opt. Lett. **39**, 6009 (2014).
23. G. Lin, S. Diallo, K. Saleh, R. Martinenghi, J.-C. Beugnot, T. Sylvestre, and Y. K. Chembo, Appl. Phys. Lett. **105**, 231103 (2014).
24. G. Lin and Y. K. Chembo, Opt. Express **23**, 1594 (2015).
25. T. Carmon, L. Yang, and K. Vahala, Opt. Express **12**, 4742 (2004).
26. M. J. Weber, *Handbook of Optical Materials* (CRC Press, 2002), Vol. **19**
27. S. Diallo, G. Lin, and Y. K. Chembo, Opt. Lett. **40**, 3834 (2015).
28. G. Lin, Y. Candela, O. Tillement, Z. Cai, V. Lefèvre-Seguin, and J. Hare, Opt. Lett. **37**, 5193 (2012).
29. D. van der Marel and H. W. den Hartog, Phys. Rev. B **25**, 6602 (1982).
30. Q.-F. Yang, X. Yi, K. Y. Yang, and K. J. Vahala, "Stokes solitons in optical microcavities," arXiv:1606.05259 (2016).
31. T. Herr, V. Brasch, J. Jost, C. Wang, N. Kondratiev, M. Gorodetsky, and T. Kippenberg, Nat. Photonics **8**, 145 (2013).
32. M. Karpov, H. Guo, A. Kordts, V. Brasch, M. H. P. Pfeiffer, M. Zervas, M. Geiselmann, and T. J. Kippenberg, Phys. Rev. Lett. **116**, 103902 (2016).
33. G. Lin, B. Qian, F. Oručević, Y. Candela, J.-B. Jager, Z. Cai, V. Lefèvre-Seguin, and J. Hare, Opt. Lett. **35**, 583 (2010).
34. I. S. Grudinin, K. Mansour, and N. Yu, Opt. Lett. **41**, 2378 (2016).
35. C. Lecaplain, C. Javerzac-Galy, M. Gorodetsky, and T. Kippenberg, "Mid-infrared ultra-high-Q resonators based on fluoride crystalline materials," arXiv:1603.07305 (2016).
36. A. Coillet, J. Dudley, G. Genty, L. Larger, and Y. K. Chembo, Phys. Rev. A **89**, 013835 (2014).
37. A. Coillet and Y. K. Chembo, Chaos **24**, 013113 (2014).
38. J. Pfeifle, A. Coillet, R. Henriet, K. Saleh, P. Schindler, C. Weimann, W. Freude, I. V. Balakireva, L. Larger, C. Koos, and Y. K. Chembo, Phys. Rev. Lett. **114**, 093902 (2015).